JACS
JOURNAL OF THE AMERICAN CHEMICAL SOCIETY

Article

pubs.acs.org/JACS

Substitution of Proline32 by α-Methylproline Preorganizes β2-Microglobulin for Oligomerization but Not for Aggregation into Amyloids

Vladimir Torbeev,[†,§] Marc-Olivier Ebert,[†] Jozica Dolenc,[‡,∥] and Donald Hilvert*[,†]

[†]Laboratory of Organic Chemistry and [‡]Laboratory of Physical Chemistry, ETH Zurich, Zurich CH-8093, Switzerland

Supporting Information

ABSTRACT: Conversion of soluble folded proteins into insoluble amyloids generally proceeds in three distinct mechanistic stages: (1) initial protein misfolding into aggregation-competent conformers, (2) subsequent formation of oligomeric species and, finally, (3) self-assembly into extended amyloid fibrils. In the work reported herein, we interrogated the amyloidogenesis mechanism of human β2-microglobulin (β2m), which is thought to be triggered by a pivotal *cis*−*trans* isomerization of a proline residue at position 32 in the polypeptide, with nonstandard amino acids. Using chemical protein synthesis we prepared a β2m analogue in which Pro32 was replaced by the conformationally constrained amino acid α-methylproline (MePro). The strong propensity of MePro to adopt a *trans* prolyl bond led to enhanced population of a non-native [*trans*-MePro32]β2m protein conformer, which readily formed oligomers at neutral pH. In the presence of the antibiotic rifamycin SV, which inhibits amyloid growth of wild-type β2m, [MePro32]β2m was nearly quantitatively converted into different spherical oligomeric species. Self-assembly into amyloid fibrils was not observed in the absence of seeding, however, even at low pH (<3), where wild-type β2m spontaneously forms amyloids. Nevertheless, we found that aggregation-preorganized [MePro32]β2m can act in a prion-like fashion, templating misfolded conformations in a natively folded protein. Overall, these results provide detailed insight into the role of *cis*−*trans* isomerization of Pro32 and ensuing structural rearrangements that lead to initial β2m misfolding and aggregation. They corroborate the view that conformational protein dynamics enabled by reversible Pro32 *cis*−*trans* interconversion rather than simple population of the *trans* conformer is critical for both nucleation and subsequent growth of β2m amyloid structures.

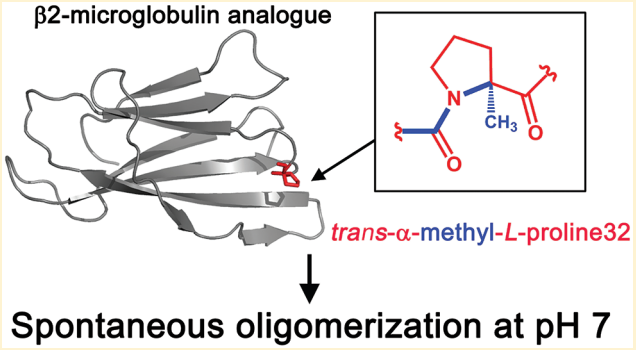

INTRODUCTION

Amyloid deposits are a pathological hallmark of a number of human diseases, including Alzheimer's, Parkinson's, and prion diseases.[1,2] Both amyloid fibers and their oligomeric precursors are believed to be the causative agents of these degenerative disorders.[3] Protein aggregation associated with amyloidoses disrupts function because the insoluble deposits directly harm cells and tissues or because molecules sequestered within the aggregates are unable to carry on their required functions.[3] Oligomeric assemblies may also interfere with specific receptors or intercalate nonspecifically into cell membranes, causing permeabilization.[4]

β2-Microglobulin (β2m) is a 99-residue human protein implicated in dialysis-related amyloidosis.[5] β2m is the light chain of major histocompatibility complex I (MHC I)[6] present on the surface of almost all cells; it also circulates in plasma in free form upon dissociation from MHC I and is catabolized in kidneys. In kidney disease patients undergoing chronic dialysis treatment, plasma clearance of β2m is disrupted, and the concentration of β2m increases up to 60-fold.[7,8] Such circumstances favor the slow accumulation of β2m as insoluble amyloid deposits in joints and connective tissues, invariably leading to medical complications.[7−9]

Elevated serum concentrations of β2m alone do not fully explain the onset of amyloid precipitation. In vitro studies have shown that wild-type (wt) β2m is soluble and monomeric in aqueous buffer at neutral pH when incubated at concentrations more than 100 times higher than those found in dialysis patients.[10,11] Systematic screening of additives identified various biological substances that enhance β2m aggregation in vitro and may contribute to amyloid formation in vivo. These include glycosaminoglycans, proteoglycans, collagen, and Cu^{2+} (reviewed in ref 5). Abiological additives that cause partial unfolding of β2m, such as organic solvents (trifluoroethanol[12]) and surfactants (sodium dodecyl sulfate[13]), also promote amyloidogenicity in vitro. Detailed studies of the mechanism of amyloid formation suggest that such factors tend to increase the concentration of a partially unfolded intermediate in which the normally *cis*-configured proline residue at position 32 in the polypeptide chain is isomerized to a *trans*-amide.[14,15]

Received: October 1, 2014
Published: January 29, 2015

DOI: 10.1021/ja510109p
J. Am. Chem. Soc. 2015, 137, 2524−2535

Scheme 1. β2-Microglobulin: Complexation with the Major Histocompatibility Complex α-Chain Versus Pathological Aggregation into Amyloid Fibrils

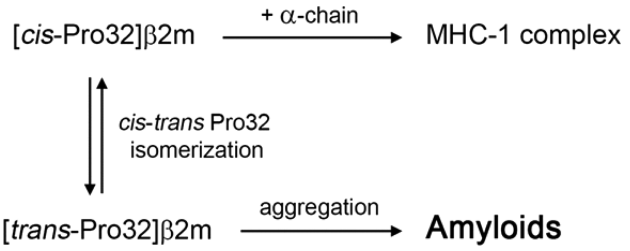

Amyloid fibrils readily self-assemble from acid-unfolded β2m at pH < 3.[16] Recent solid-state NMR studies showed that these amyloids contain a *trans*-configured Pro32.[17,18] Although this is not the only structural change associated with amyloid formation (the topology of the β-sheets in the protein also changes from antiparallel in native β2m to parallel in the amyloids[18,19]), the *cis*−*trans* isomerization of Pro32 has been suggested to trigger the transition of soluble, monomeric β2m to misfolded, amyloidogenic species (Scheme 1).[20,21] Indeed, slow *cis*−*trans* isomerization of proline residues has been shown to induce large-scale global structural changes in other proteins and protein complexes, providing a simple molecular mechanism for biological regulation.[22]

Data on ΔN6, a β2m variant that lacks the first six N-terminal residues, support the hypothesis that the *trans*-Pro32 conformer promotes protein aggregation.[11,23] Truncation of β2m destabilizes the *cis*-Pro32 conformer to such an extent that only *trans*-Pro32 is observed by NMR at neutral pH.[23] Moreover, the ΔN6 variant is more dynamic than wt β2m and self-assembles as amyloids under physiological conditions.[23,24] Solid-state NMR studies of the resulting fibrils confirmed that Pro32 adopts a *trans* configuration as in wt amyloids.[25] Nevertheless, studies on β2m variants in which Pro32 was mutated to glycine, alanine or valine indicate that constraining residue 32 to a *trans* configuration alone is not sufficient to induce amyloid formation.[14,15] Each of these mutations would be expected to increase the fraction of *trans* amide (>99.9% in short peptides) relative to native proline, but only the Pro32Gly substitution yielded a protein capable of forming fibers in seeding experiments.[21] The other two variants did not nucleate fibril formation or elongate amyloid fibrillar seeds.[20,21,26] Even though acyclic amino acids favor formation of a *trans*-His31-Xaa32 peptide bond, they only imperfectly mimic the unique backbone conformations imposed by the five-membered pyrrolidine ring of native proline and the conformational dynamics made possible by relatively facile *cis*−*trans* isomerization of the proline amide bond.[15]

We recently reported the total chemical synthesis of wt β2m and used this approach to construct three chemical analogues containing either (2*S*,4*S*)-4-fluoroproline, (2*S*,4*R*)-4-fluoroproline or 4,4-difluoroproline in place of Pro32.[27] These fluorinated proline derivatives, which are nearly isosteric to the natural amino acid and share similar conformational properties, were used to modulate protein stability and amyloidogenicity by systematically altering the *cis*/*trans* equilibrium configuration of residue 32. As expected, substitution of Pro32 with (2*S*,4*S*)-4-fluoroproline, which favors the *cis*-amide isomer,[28] stabilized the native protein conformation in chemical denaturation experiments, whereas introduction of (2*S*,4*R*)-4-fluoroproline, which has a higher tendency to populate the *trans* isomer,[28] destabilized the protein. Nevertheless, in the absence of denaturant, incorporation of (2*S*,4*R*)-4-fluoroproline did not lead to significant population of the *trans*-prolyl conformer at neutral pH. Destabilization of this protein variant was evidently insufficient to trigger oligomerization and self-assembly into amyloid structures. Unexpectingly, the most readily aggregating protein variant in this series contained a 4,4-difluoroproline at position 32. This residue has a *cis*/*trans* equilibrium amide bond propensity similar to unmodified proline, but the rate of *cis*−*trans* isomerization is higher (nearly 10-fold at 37 °C in Ac-Xaa-OMe model compounds[28]). The 4,4-difluoroproline-containing variant spontaneously oligomerized at neutral pH upon incubation for several weeks, but yielded amorphous protein aggregates rather than amyloids. In this protein analogue, oligomers effectively served as a kinetic trap for rapidly unfolding conformers. At low pH (<3), like wt β2m, all fluoroproline-containing β2m analogues formed amyloids, albeit as distinct polymorphs. Together, these observations provided support for the hypothesis that *cis*−*trans* isomerization of Pro32 underpins amyloid self-assembly, yet also highlighted the importance of protein conformational dynamics in this process.[27]

In this paper, we extend our investigations into the role of Pro32 isomerization in β2m aggregation by replacing this residue with α-methyl-L-proline (MePro). Like fluoroprolines, MePro has a five-membered pyrrolidine ring structure. However, the steric demands of the additional α-methyl group cause a more pronounced preference for the *trans*-amide conformer.[29−34] The free energy barrier for *cis*−*trans* isomerization is also higher than with proline.[35] As a consequence, only the *trans* isomer is populated in short isotactic (homochiral) peptides containing MePro with backbone φ/ψ-dihedral angles favoring a $3_{10}/\alpha$-helical conformation.[30−35] We anticipated that replacing Pro32 with this highly conformationally constrained amino acid might similarly override the normal contextual bias of the BC loop structure in natively folded β2m[36] and populate the aggregation-prone *trans*-prolyl amide conformer. Here we report the chemical synthesis of the [MePro32]β2m variant, as well as its biophysical characterization and aggregation properties.

RESULTS

Molecular Dynamics Simulations Show That the *trans* and *cis* Conformers of [MePro32]β2m Have Distinct Structural and Dynamic Properties. To gain insight into the structural perturbations that introduction of α-methylproline at position 32 of β2m might cause, we performed all-atom explicit solvent molecular dynamics (MD) simulations on both the [*cis*-MePro32]β2m and [*trans*-MePro32]β2m conformers for 60 ns. Although the overall tertiary structures of these conformers are similar, the two species exhibit substantial differences in detail, as seen in the superposition shown in Figure 1A,B. An analysis of backbone root-mean-square fluctuations (RMSF) revealed increased fluctuations for residues 14−19, 28−37, and 52−59 in the [*trans*-MePro32]-β2m conformer (Figure 1C), indicating that structural changes associated with the MePro32 residue not only influence the conformation of nearby residues but also induce conformational changes in more distant loops. The increased flexibility of [*trans*-MePro32]β2m is also reflected in the higher atom-positional root-mean-square deviations (RMSD) of the backbone atoms from the respective energy-minimized initial

DOI: 10.1021/ja510109p
J. Am. Chem. Soc. 2015, 137, 2524−2535

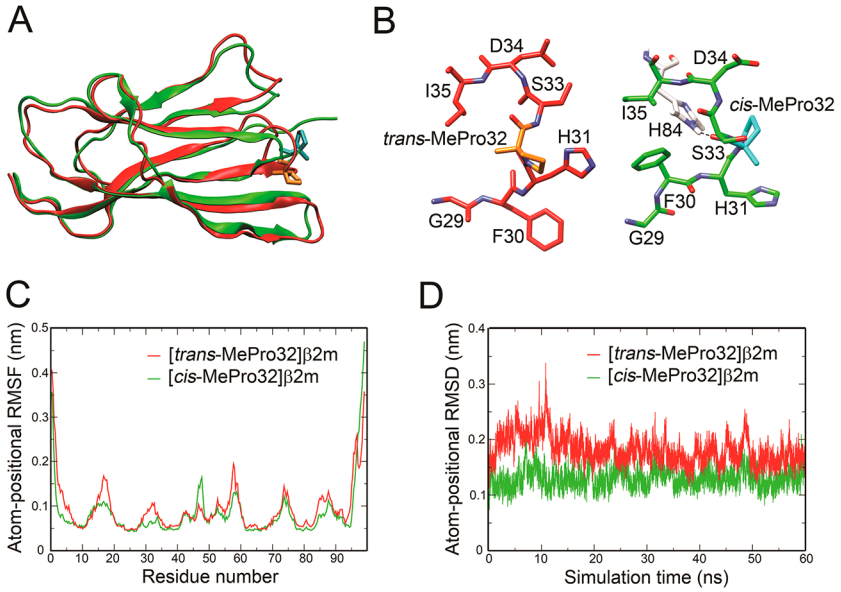

Figure 1. Molecular dynamics simulations of *trans*- and *cis*-MePro32 conformers of [MePro32]β2m (MePro = α-methyl-L-proline). (A) Overlay of [*trans*-MePro32]β2m (red) and [*cis*-MePro32]β2m (green) with the MePro32 residue shown in orange and cyan, respectively. Superposition was done using backbone atoms. The depicted conformations are central-member structures of the most populated clusters obtained from 60 ns explicit solvent MD simulations and represent approximately 95% of the [*cis*-MePro32]β2m ensemble and 86% of the [*trans*-MePro32]β2m ensemble. Both proteins were simulated with the GROMOS 54A7 force field at 300 K. (B) A close-up view of the BC loop structure, which contains residue 32, shows that an NH(ε)···O hydrogen bond forms between His84 (shown in gray) and MePro32 in the [*cis*-MePro32]β2m conformer but not in the [*trans*-MePro32]β2m conformer. (C) Root-mean-square fluctuations of the backbone atoms (N, C, Cα) for the [*trans*-MePro32]β2m (red) and [*cis*-MePro32]β2m (green) simulations. (D) Time series of the backbone atom-positional root-mean-square deviation from the initial structure for the [*trans*-MePro32]β2m (red) and [*cis*-MePro32]β2m (green) simulations. See Table S1 and Figures S1 and S2 for analyses of hydrogen bonding patterns, the persistence of secondary structure elements as a function of time, and His31-MePro32 Cα−N−C−C′α dihedral angles in the simulations of [MePro32]β2m.

structures as shown in Figure 1D. While the RMSD remained below 0.22 nm (with a mean value of 0.13 nm) in the MD simulation of [*cis*-MePro32]β2m, the corresponding values for [*trans*-MePro32]β2m ranged up to 0.34 nm (with a mean value of 0.18 nm).

Additional insights into the structural differences between [*trans*-MePro32]β2m and [*cis*-MePro32]β2m were gained from hydrogen bond analysis. As seen in the complete list of hydrogen bonds provided in Table S1, the two conformers exhibit distinctive hydrogen-bonding patterns. For example, in the simulations of [*trans*-MePro32]β2m, the MePro32 residue did not engage in any significant hydrogen bonding interactions with the rest of the protein. In contrast, in [*cis*-MePro32]β2m, a hydrogen bond between the carbonyl group of MePro32 and NH(ε) of the imidazole ring of His84 persisted for more than 92% of the simulation (Figure 1B), as found previously in MD simulations of the wt protein.[36]

Comparison of the MD simulations for the two amide32 isomers of [MePro32]β2m and wt β2m further showed that introduction of the α-methyl group generally lowered the RMSD and RMSF values for the *trans* and *cis* conformers (see Figure S3), in agreement with the constraining properties of MePro. A detailed analysis of the φ/ψ-dihedral angles and ring puckering for residue 32 in the MD simulations for [MePro32]β2m and wt β2m revealed that the conformational preferences of the MePro32 and Pro32 residues are distinct (Figure S4). Differences are especially pronounced for *trans*-MePro32 and *trans*-Pro32, where the former mostly populates a $3_{10}/\alpha$-helical conformation, whereas the latter adopts φ/ψ-angles corresponding to a polyproline type II (PPII) helix.

Incorporation of α-Methylproline into β2m Populates a Non-native Conformer, Destabilizes the Protein, and Leads to Oligomerization at Neutral pH. Chemical synthesis of [MePro32]β2m was carried out using one-pot native chemical ligation of three polypeptide fragments as previously described.[27] After formation of the Cys25−Cys80 disulfide bond by air-oxidation, the [1−99]peptide product was purified to homogeneity by reverse-phase HPLC (for analytical data see Figure S5). It was subsequently folded by dialysis against sodium phosphate buffer at pH 7.5, and isolated by size exclusion chromatography (SEC). Monomeric [MePro32]β2m eluted as a mixture of two poorly separated components rather than as a single symmetric peak (Figure 2 A).

To characterize these species, we prepared and purified two labeled versions of the protein (Table S2). In the first construct, the α-methyl group of the MePro residue was uniquely ^{13}C-labeled. In the second, amides of nine residues (Ile7, Val9, Ala15, Gly18, Phe22, Val27, Gly29, Phe30, and Ile35) were labeled with ^{15}N. In agreement with the SEC data, proton-detected ^{13}C and ^{15}N HSQC spectra confirmed the presence of two components (or conformers) in the sample (Figure 2B,C). Thus, two major peaks were observed in the ^{1}H−^{13}C HSQC spectrum for the [$^{13}CH_3$Pro32]β2m variant in an approximately 64:36 ratio (Figure 2B). Based on the ^{13}C NMR chemical shift (^{13}C, δ = 20.1 ppm) of the α-methyl group in a MePro-containing peptide (Ac-Phe-His-MePro-Ser-Asp.NH_2), we assigned the major peak to the *trans*-MePro32 conformer (^{13}C, δ = 20.2 ppm) and the minor peak tentatively to *cis*-MePro32 (^{13}C, δ = 24.4 ppm). Similarly, the ^{1}H−^{15}N HSQC spectrum of the ^{15}N-labeled construct showed doublets for residues that are either in close proximity to MePro32 (Gly29,

DOI: 10.1021/ja510109p
J. Am. Chem. Soc. 2015, 137, 2524−2535

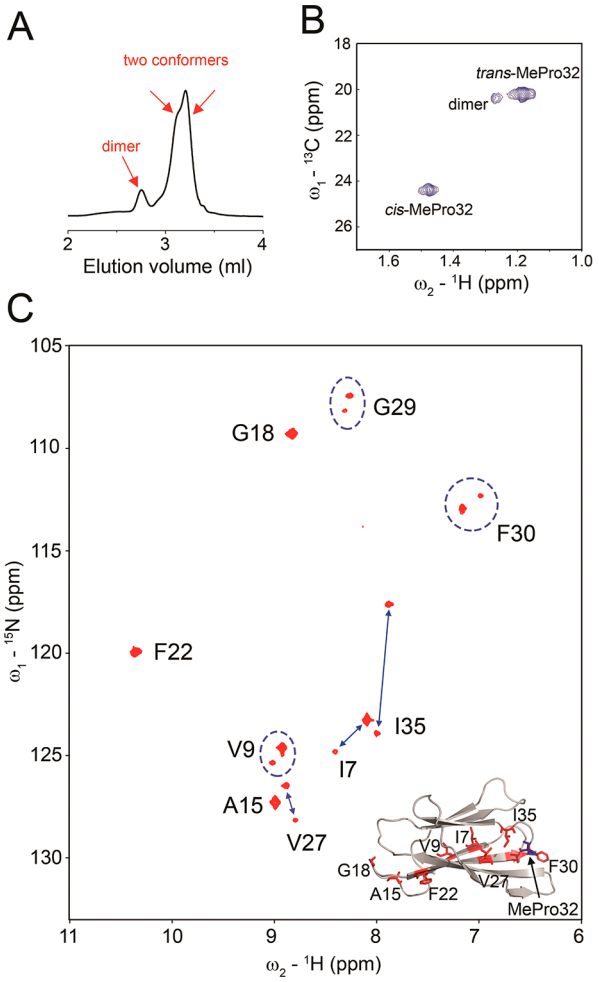

Figure 2. NMR spectra of ^{13}C- and ^{15}N-isotope-labeled [MePro32]-β2m variants. (A) Size-exclusion HPLC (SEC) of freshly folded [MePro32]β2m shows a monomer peak that is composed of two components (conformers) plus a peak corresponding to a dimeric species. See Figure 4 for chromatograms showing time-dependent aggregation of [MePro32]β2m and wt β2m. (B) ^{1}H−^{13}C HSQC of α-[^{13}CH$_3$]Pro32-labeled [MePro32]β2m shows the presence of three species (*trans*- and *cis*-MePro32 conformers plus the dimeric species) in qualitative agreement with the SEC data. (C) ^{1}H−^{15}N HSQC spectrum of ^{15}N-labeled [MePro32]β2m (locations of labels are mapped in red and displayed as in inset in the right bottom corner). Residues Ala15, Gly18, and Phe22 show single amide resonances with chemical shifts identical to the corresponding signals in wt β2m (overlay of ^{1}H−^{15}N HSQC spectra for [MePro32]β2m and corresponding chemical shifts measured for wt β2m[23] are depicted in Figure S6). All other residues Ile7, Val9, Val27, Gly29, Phe30, and Ile35 show two signals, corresponding to *trans* and *cis* conformers of [MePro32]β2m, respectively. Pairwise assignments (signals that are encircled or connected by blue lines) were made on the basis of similarities in the chemical shifts, except for Ile35 and Ile7, where the assignments are ambiguous.

Phe30, Ile35) or located in the hydrophobic core of the protein (Val27, Ile7, Val9) (Figure 2C). In contrast, three residues (Ala15, Gly18, Phe22) that are more distant from MePro32 gave single peaks with chemical shifts identical to those of the corresponding peaks in the wt β2m spectrum.[23] Figure S6 shows the ^{1}H−^{15}N HSQC spectrum for [MePro32]β2m overlaid on the previously reported spectrum for wt β2m.[23] The less populated conformer had ^{1}H−^{15}N chemical shifts either identical or very similar to the peaks observed in the spectrum of wt β2m in agreement with the assignment of these species to the [*cis*-MePro32]β2m conformer and consistent with a structure very close to that of wt β2m. Small differences in chemical shift values for residues Val27, Gly29, and Phe30 are likely due to the slightly altered conformational properties of nearby *cis*-MePro32 versus *cis*-Pro32, as observed in the corresponding MD simulations (Figure S4). In contrast, the chemical shifts for the more dominant conformer showed significant deviations from wt β2m, suggesting more pronounced structural perturbations in line with the MD simulations of [*trans*-MePro32]β2m.

Direct NMR detection of two distinct conformers for [MePro32]β2m reflects the slow rate of conformational exchange on the NMR time scale and the intrinsically high free energy barrier for *cis*−*trans* isomerization of the MePro residue. The data suggest that roughly 40% of the protein adopts a wild-type-like structure, with MePro32 in a *cis* conformation, whereas as the remaining ∼60%, containing a *trans*-configured MePro32, shows significant structural deviations. Thus, the inherent conformational preferences of the MePro residue are able to override the normal contextual preferences of the BC loop to a significant extent.

Population of the *trans*-MePro32 amide appears to loosen the protein structure. Increased flexibility is manifest in the greater susceptibility of [MePro32]β2m to tryptic digestion (see Figures 3A, S7, and S8) as well as in enhanced binding to the environmentally sensitive dye 8-anilino-1-naphthalenesulfonic acid (ANS) (Figure 3B). Moreover, the thermal stability of [MePro32]β2m is significantly reduced with an apparent melting temperature (T_m) of 52 °C versus 61.5 °C for wt β2m (Figure 3D). Finally, the less compact structure of [MePro32]-β2m variant is also reflected in the ^{1}H NOESY spectrum, which shows fewer HN-HCα NOE peaks than the corresponding spectrum for wt β2m (Figure 3E,F).

The circular dichroism spectrum of [MePro32]β2m is also distinctly different from that of wt β2m, with a diminished maximum at 203 nm and a blue-shifted minimum at 218 nm (Figure 3C). These spectral features are a common signature of aggregating β2m variants.[11] In fact, facile oligomerization of [MePro32]β2m was observed at neutral pH. In contrast to wt β2m, which does not aggregate under these conditions, dimeric species were detected in size exclusion chromatograms of freshly folded [MePro32]β2m (Figure 4). Incubation of the sample for several days yielded even higher molecular weight species eluting in the void volume of the size-exclusion column (Figure 4). This conglomerate proved to be relatively stable as further progression to amyloid fibrils was not observed over several weeks at neutral pH.

Amyloidogenic Properties of [MePro32]β2m and Chemical Analogues. Wild-type β2m spontaneously forms long, straight amyloids at pH 2.5 with or without agitation.[16] In contrast, despite readily forming oligomers at neutral pH, [MePro32]β2m did not form amyloid fibrils, even upon prolonged incubation (up to 1 month) at pH 2.5. Instead, amorphous aggregates were obtained (Figure 5A).

To gain further insight into how local conformational flexibility of residue 32 influences β2m amyloidogenicity, we chemically synthesized the previously studied Pro32Gly β2m analogue[21,37] as well as a new variant, in which Pro32 was substituted by α-aminoisobutyric acid (Aib) (Table S2 and Figure S9). In the Pro32Gly variant, Gly32 can sample a wide range of conformations in Ramachandran φ/ψ space, whereas Aib is achiral, like glycine, but conformationally constrained

DOI: 10.1021/ja510109p
J. Am. Chem. Soc. 2015, 137, 2524−2535

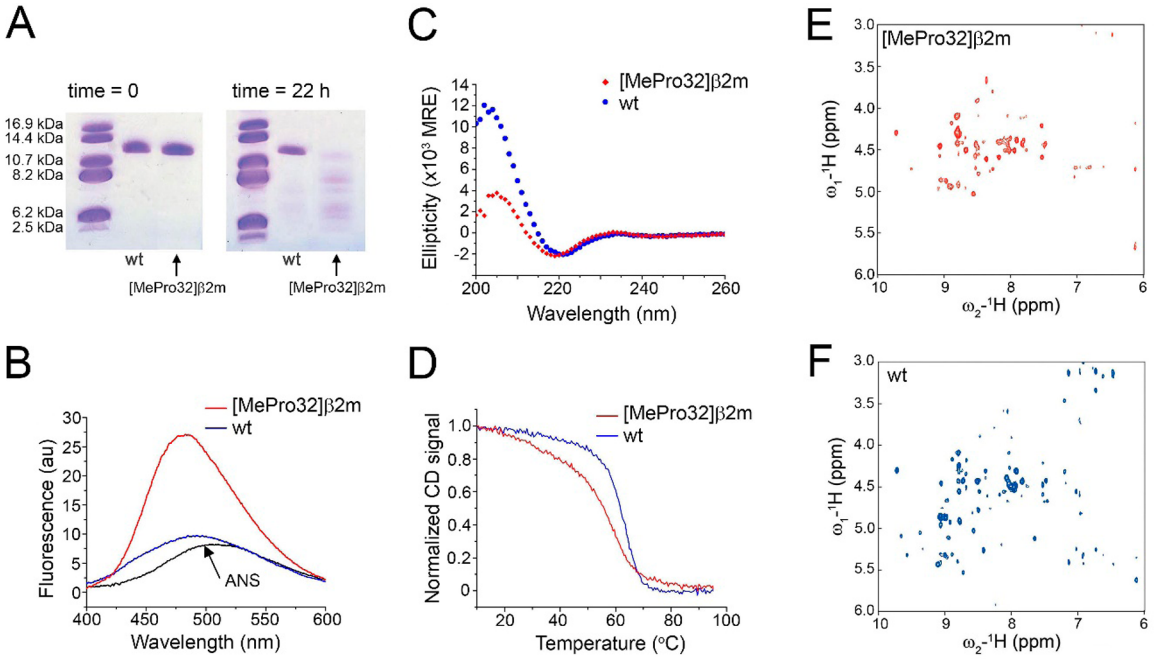

Figure 3. Properties of chemically synthesized [MePro32]β2m and wt β2m. (A) Protein stability against tryptic digestion monitored by SDS-PAGE (see Figures S7 and S8 for corresponding HPLC data). (B) Fluorescence of ANS dye [concentration (c) 10 μM] upon addition of either [MePro32]β2m or wt β2m ([protein] = 2 μM). The spectrum of ANS in the absence of protein is shown in black. (C) Far-UV CD-spectra of [MePro32]β2m (in red) and wt β2m (in blue) recorded at 37 °C. (D) Thermal denaturation monitored by CD spectroscopy reveals less cooperative melting for [MePro32]β2m with an apparent T_m of 52 °C versus 61.5 °C for wt β2m. (E,F) ^{1}H-NOESY NMR spectra of [MePro32]β2m and wt β2m, respectively. Conditions for spectra acquisition: for [MePro32]β2m, 64 FIDs/increment, [protein] = 0.3 mM; for wt β2m, 16 FIDs/increment, [protein] = 0.35 mM. Regions corresponding to HN−HCα NOEs are shown. The [MePro32]β2m variant shows a smaller number of NOEs and reduced peak dispersion compared to wt β2m, which indicates that [MePro32]β2m is less structured.

similar to α-methylproline. Both Gly and Aib residues strongly favor a *trans*-amide conformation. Incubation of the samples at pH 2.5 yielded curvilinear aggregates in the case of [Gly32]β2m and amorphous aggregates for [Aib32]β2m (Figure S10) rather than the long straight fibers observed for wt β2m.[16]

The addition of preformed wt amyloid seeds to the acid-denatured proteins dramatically changed the outcome of the fibrilization experiments. The [MePro32]β2m analogue, as well as the [Gly32]β2m and [Aib32]β2m variants, readily formed amyloid fibrils, albeit at slower rates than wt β2m (see Figures 5, S11, and S12). These results indicate that the distinct conformational and dynamic properties of MePro, Gly, and Aib do not significantly affect the ability of the corresponding proteins to integrate onto the surface of preformed amyloid seeds. However, replacement of Pro32 by these three residues drastically alters the ability of the corresponding protein variants to nucleate amyloid self-assembly.

Rifamycin SV Diverts the Oligomerization Pathway of [MePro32]β2m at Neutral pH. Previously, screening of small molecule libraries identified rifamycin SV (RifSV) as an inhibitor of β2m amyloid growth at low pH.[38] It was shown that RifSV binds to acid-unfolded β2m conformers and induces formation of spherical oligomers.[38] We consequently investigated the effect of RifSV on [MePro32]β2m oligomerization.

Dialysis of [MePro32]β2m at neutral pH in the presence of RifSV led to formation of oligomers with a molecular weight distribution distinct from that observed for [MePro32]β2m alone. Thus, incubation of the mixture for 2 weeks resulted in complete conversion of monomeric protein to oligomeric species (Figure 6A,B). Control experiments with wt β2m under the same conditions also yielded oligomers but in significantly lower amounts. These results suggest that RifSV interacts primarily with the *trans*-Pro32 conformer, which is abundant in the case of [MePro32]β2m but not significantly populated in wt β2m at pH 7.5 (Figure S13).

Size-exclusion chromatography, monitored at 450 nm (the characteristic absorption band of RifSV), demonstrated that RifSV binds directly to the protein oligomers (Figure 6B). Binding is noncovalent since protein adducts were not observed when denatured samples were analyzed by mass spectrometry. Similar to the results obtained for wt β2m at pH 2.5 in the presence of RifSV,[38] TEM showed that the RifSV-induced [MePro32]β2m oligomers were spherical particles of heterogeneous size (Figure 6C). The circular dichroism spectrum of the sample indicated that [MePro32]β2m is disordered (unstructured) in these aggregates (Figure 6D).

The dramatic structural changes caused by RifSV are further illustrated by ^{1}H−^{15}N TROSY data (Figure 6E). Initially, only small chemical shift changes were observed for residue Phe22 in ^{15}N-labeled [MePro32]β2m upon addition of RifSV. However, incubation of the sample for 2 weeks led to a completely different spectrum with substantially reduced chemical shift dispersion.

These results provide strong evidence for a disordered [MePro32]β2m structure in the oligomers (Figure 6E). In essence, this system constitutes a clear case of small-molecule-induced protein misfolding.

[MePro32]β2m Templates an Aggregation-Prone Conformation in a Natively Folded Protein. The finding that [MePro32]β2m does not produce amyloids at pH 2.5 suggests that substitution of proline by MePro somehow hinders structural rearrangements in the monomer that may be

DOI: 10.1021/ja510109p
J. Am. Chem. Soc. 2015, 137, 2524−2535

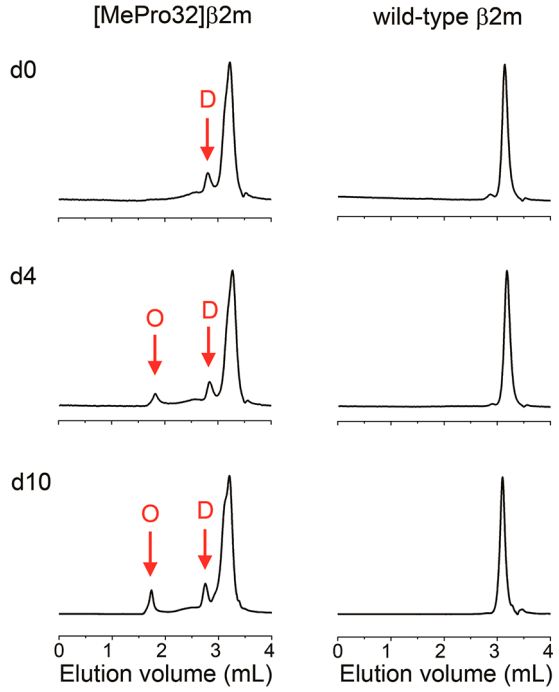

Figure 4. Monitoring aggregation of [MePro32]β2m and wt β2m by size-exclusion chromatography (SEC). Chromatograms of [MePro32]β2m (left column) and wt β2m (right column) measured immediately after completion of the folding reaction (d0), after 4 day incubation (d4), and after 10 day incubation (d10) at 25 °C. [MePro32]β2m readily forms dimers and oligomers, whereas wt β2m protein is stable in monomeric form ([protein] = 40 μM). In the left column, D stands for dimer and O stands for high-order oligomers. Column was size-calibrated with protein standards prior to measurements.

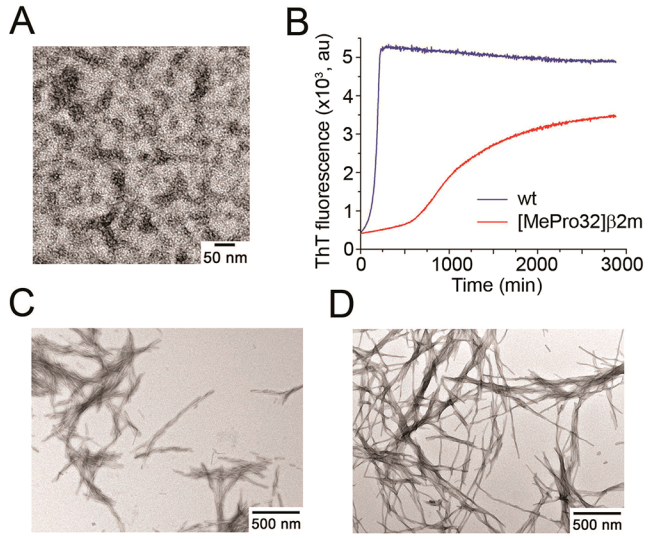

Figure 5. Aggregation properties of [MePro32]β2m protein. (A) Oligomers formed from [MePro32]β2m incubated at 50 μM concentration in 50 mM citrate buffer, 100 mM NaCl, pH 2.5, for 2 weeks at 37 °C with shaking (250 rpm). (B) Kinetics of amyloid growth for wt β2m and [MePro32]β2m upon seeding with preformed wt β2m amyloid seeds in 50 mM citrate buffer, 100 mM NaCl, pH 2.5 at 27 °C. TEM images of (C) wt β2m amyloids and (D) [MePro32]β2m upon completion of the experiment shown in (B).

required to produce amyloid-like nuclei needed for fibril formation.[39] Given the similarity of proline and MePro, the likely explanation for these findings is the greater local rigidity at position 32 arising from the conformational constraints imposed by the extra α-methyl group. Although [MePro32]-β2m is oligomerization-prone, aggregation terminates at the stage of oligomers that are resistant to further rearrangement and/or self-assembly into amyloid-like structures.

While MePro approximates the structure and conformation of native proline better than any other ribosomally encoded amino acid, it is still an imperfect replacement. The additional α-methyl group leads to a stronger preference for a *trans*-amide and a higher *cis*–*trans* isomerization barrier, but it also modifies the conformational propensities of the amino acid, in particular around the ψ-torsional angle (see Figure S4 and refs 31–34). The latter properties may contribute to the altered aggregation behavior of the [MePro32]β2m analogue. However, because similar amyloid growth was observed for [Gly32]β2m and [Aib32]β2m (see above), two variants that also contain a *trans*-amide32 but quite different φ/ψ-conformational preferences, *cis*–*trans* isomerization is likely to be the critical factor influencing oligomerization.

We reasoned that the decreased local flexibility of α-methylproline might predispose [MePro32]β2m to serve as a template for conversion of folded native β2m into an aggregation-prone conformation. In principle, the *trans*-[MePro32]β2m conformer might function like prion species[40] and catalyze the *cis*–*trans* interconversion of Pro32 in β2m. To test this hypothesis, we used the previously characterized [F_2Pro32]β2m[27] as a surrogate for wt β2m. Like Pro32 in wt β2m, F_2Pro32 adopts a *cis* conformation in freshly prepared samples of [F_2Pro32]β2m,[27] but due to the lower free energy barrier for *cis*–*trans* isomerization of the F_2Pro residue,[28] the [F_2Pro32]β2m protein is more plastic than wt β2m with respect to conformational interconversion. Conveniently, it is also possible to monitor the *cis*–*trans* isomerization of the F_2Pro32 residue directly by 1D ^{19}F NMR spectroscopy.

Figure 7A shows the ^{19}F NMR spectrum of [F_2Pro32]β2m after folding by dialysis at neutral pH. As expected, only the *cis*-F_2Pro conformer is observed. The pair of doublets belongs to an AB nuclear spin system consisting of two magnetically nonequivalent geminal fluorine atoms with a spin coupling constant ^2J = 235 Hz. Based on analogous ^{19}F NMR data for a model pentapeptide,[27] this pattern indicates that the F_2Pro residue adopts a *cis* amide conformation.

The freshly prepared [F_2Pro32]β2m sample was mixed with [MePro32]β2m in a 1:1 ratio and stored at 37 °C. Remarkably, after a 2 month incubation, additional peaks corresponding to the *trans*-F_2Pro32 conformer emerged (Figure 7C, 20% *trans*-F_2Pro32 upon integration). A control sample of [F_2Pro32]β2m alone at a 2-fold higher protein concentration yielded a much smaller percentage of the *trans*-F_2Pro32 isomer (Figure 7D, 6% *trans*-F_2Pro32 upon integration). This result unambiguously demonstrates prion-like transmission from [MePro32]β2m to [F_2Pro32]β2m and stabilization of an aggregation-prone conformation.

Analysis of the two samples by size-exclusion chromatography showed distinct differences in the composition of soluble oligomers (Figures 7E,F). While TEM analysis did not reveal long straight amyloids in either sample (Figure S14), a thioflavin T (ThT) assay[41] gave a higher fluorescence response for the [MePro32]β2m:[F_2Pro32]β2m mixture than for the [F_2Pro32]β2m sample, which may be indicative of higher cross-β structural content in the mixture (Figure 7B).

DOI: 10.1021/ja510109p
J. Am. Chem. Soc. 2015, 137, 2524–2535

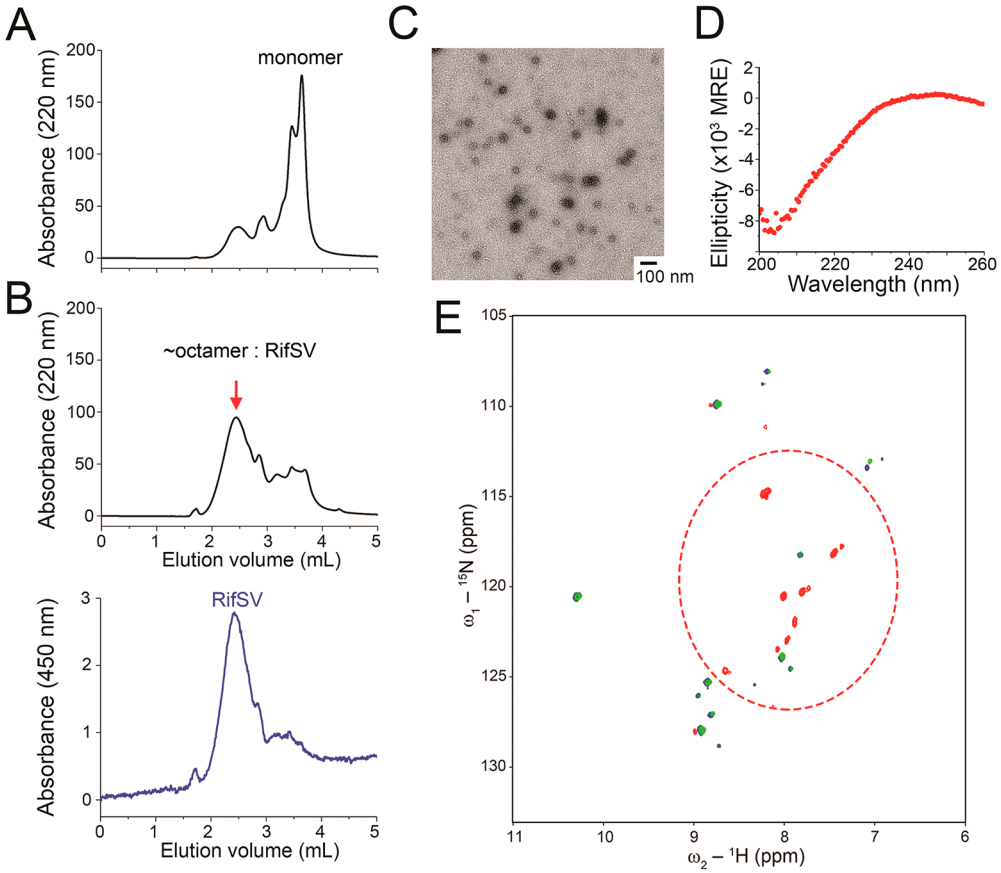

Figure 6. Rifamycin SV (RifSV) induces oligomerization of [MePro32]β2m at neutral pH. (A) Size-exclusion chromatogram after folding by dialysis in the presence of RifSV (for 3 days, 3 kDa molecular weight cutoff membrane). (B) After 2 week incubation at pH 7.3, 37 °C the chromatogram is dominated by a broad peak with a retention time approximately corresponding to an [MePro32]β2m octamer. Complementary measurement at λ = 450 nm indicates that RifSV is bound to the protein oligomer. (C) TEM images revealed distributions of spherical oligomers of heterogeneous size. (D) The CD spectrum of the [MePro32]β2m–RifSV complex shows that the protein is unstructured. (E) $^{1}H-^{15}N$ TROSY spectra of [MePro32]β2m ([protein] = 250 μM) following addition of 100 μM RifSV (in blue), 750 μM RifSV (in green), and 750 μM RifSV and incubation for 2 weeks (in red).

DISCUSSION

Much experimental evidence suggests that protein misfolding occurs through metastable, partially unfolded or "alternative" conformations.[42,43] For example, prions, which can self-propagate in vivo,[40] constitute a special class of proteins that adopt transmissible misfolded states. Apart from understanding the biological properties of prion species, including infectivity and heredity, a challenge in this field is to determine the structures of these conformers at atomic resolution and to characterize their properties. Knowing such details may aid in the design of inhibitors of protein aggregation and provide tools for diagnosis and prevention of protein misfolding diseases.[40]

In the original work on prion proteins,[44] conversion of noninfectious prions (PrP^{C}) into an infectious species (PrP^{Sc}) was shown to entail a conformational isomerization involving a decrease in α-helical content and an increase in β-sheet content.[45] It was suggested that the mechanism by which PrP^{Sc} is formed must involve a templating process whereby existing PrP^{Sc} directs the refolding of PrP^{C} into a nascent PrP^{Sc} with the same conformation.[46] Various additives can also influence the conformation of PrP^{Sc}, affecting its propagation, strain properties, and infectivity.[47−49] In fact, early studies using bacterially expressed recombinant PrP alone failed to recapitulate the properties of infectious PrP^{Sc}.[50] Substantiating these findings, recent X-ray fiber diffraction data showed that recombinant PrP amyloids and highly infectious brain-derived prions have significantly different structural properties.[51]

In the case of the amyloid β (Aβ) peptide involved in Alzheimer's disease, it was similarly found that brain-derived aggregates have higher transmissibility than synthetic Aβ amyloids upon inoculation in mice brains.[52] A solid-state NMR study of Aβ amyloids generated by "seeding" with isolates taken from the brain of a deceased Alzheimer's patient identified a unique amyloid polymorph with a structure distinct from known structures of amyloids grown entirely in vitro.[53] How exactly the biological environment modulates these structures, however, remains poorly understood.

Biological additives have also been found to enhance the formation of amyloids derived from human β2m.[5,15] Collagen,[54,55] glycosaminoglycans,[56,57] proteoglycans,[58] non-esterified fatty acids,[59] lysophospholipids,[60,61] and Cu^{2+} ions[20,62,63] accelerate formation of amyloid fibrils in vitro at neutral pH. The effect of these additives can be twofold. On the one hand, they may destabilize the native state of β2m and increase the concentration of partially unfolded conformers. On the other hand, they may stabilize oligomers or fibrils against depolymerization. Although β2m amyloid fibrils grown at low pH tend to be unstable and spontaneously disintegrate upon transfer into neutral buffer,[64,65] they can be stabilized by a combination of several additives (heparin, lipoprotein E, and

DOI: 10.1021/ja510109p
J. Am. Chem. Soc. 2015, 137, 2524−2535

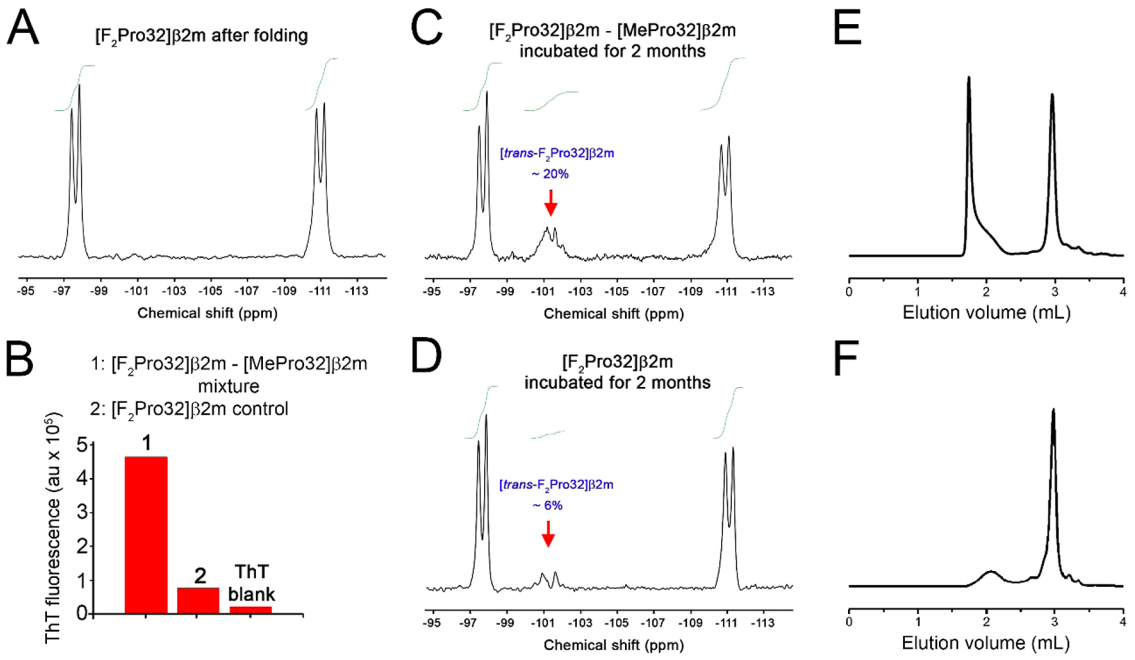

Figure 7. Addition of [MePro32]β2m accelerates accumulation of *trans*-F_2Pro32 in [F_2Pro32]β2m. (A) ^{19}F NMR spectrum of freshly prepared [F_2Pro32]β2m, (B) ThT fluorescence (λ_{ex} = 440 nm, λ_{em} = 480 nm) of the 1:1 [F_2Pro32]β2m:[MePro32]β2m mixture and [F_2Pro32]β2m after 2 months incubation at 37 °C and the solution of ThT dye only. (C) ^{19}F NMR spectrum of a 1:1 [F_2Pro32]β2m: [MePro32]β2m mixture after incubation for 2 months at 37 °C. (D) ^{19}F NMR spectrum of a [F_2Pro32]β2m after incubation for 2 months at 37 °C. Size-exclusion chromatograms of (E) the [F_2Pro32]β2m:[MePro32]β2m mixture and (F) [F_2Pro32]β2m, each after 2 months incubation. An overlay of ^{1}H−^{15}N HSQC spectra for a 1:1 [F_2Pro32]β2m:[MePro32]β2m mixture after sample preparation and after 2 months incubation is provided in Figure S15. The data are in agreement with accumulation of soluble misfolded species upon prolonged incubation.

serum amyloid P component).[66] Such mixtures have also been used to prepare "seeds" for initiating amyloid growth at neutral pH.

Additive-induced amyloidosis of native β2m has been linked to a shift in the *cis/trans* equilibrium of the His31-Pro32 amide bond in favor of the *trans*-Pro32 conformer, which is competent for oligomerization.[11,15] Using chemical protein synthesis as a tool,[67] we site-specifically replaced Pro32 with an unnatural, conformationally constrained MePro residue that has a strong preference for the *trans* prolyl configuration. Chemical strategies for studying protein misfolding have several advantages: (i) the desired conformer is conformationally stabilized and chemically isolated and, therefore, amenable to direct structural and biophysical characterization; (ii) the chemical composition and molecular interactions of the modified residue are well-defined (in contrast to mixtures of different additives); and (iii) conformational effects (i.e., properties of a particular protein conformer) are separated from the surfactant effects of additives.

Although the [MePro32]β2m variant prepared by total chemical synthesis readily formed oligomers at neutral pH (Figure 4), no amyloids were observed either at neutral pH or under the acidic conditions (pH < 3) that yield amyloid fibers of wt β2m within a few days. Only upon "seeding" with preformed wt β2m amyloids could long, straight amyloids be formed from [MePro32]β2m. The resulting fibrils are morphologically similar to those obtained with wt β2m, but not identical (see Figure 5C,D). This finding suggests that the conformational constraints imposed by MePro32, while stabilizing the *trans*-prolyl conformation and facilitating oligomerization, may hinder subsequent reorganization of the oligomers into amyloid-like precursors (nuclei) of full-length amyloids.[39] Seeding obviates the need for nucleation, but the slower kinetics of seeded amyloid growth observed for [MePro32]β2m (Figure 5B) further suggests that the constrained *trans*-MePro32 β2m conformer is not readily integrated at the growing end of the amyloid fibril. Conceivably, multiple $(trans{-}cis)_n$ isomerizations, which are possible for native proline, are needed to access the cross-β structure characteristic of amyloid fibrils. This conclusion is supported by the distinct aggregation properties of β2m analogues containing different fluoroproline derivatives in place of Pro32.[27]

The conformationally constrained nature of [MePro32]β2m facilitated investigations of its interactions with rifamycin SV, a small-molecule antibiotic that is a potent inhibitor of wt β2m amyloid growth under acidic conditions.[38] Although it was not possible to isolate or characterize the wt β2m:RifSV complex at neutral pH,[38] population of the *trans*-prolyl conformer in [MePro32]β2m allowed direct monitoring of complex formation by size-exclusion chromatography and NMR spectroscopy (Figure 6). In agreement with previous conclusions,[38] RifSV appears to trap β2m in a misfolded state that affords spherical oligomers rather than amyloids (Figure 6C). Importantly, our NMR and CD data on the [MePro32]-β2m:RifSV complex indicate that the protein molecule is disordered in this complex (see Figure 6D,E).

The high conformational stability of [*trans*-MePro32]β2m also allowed us to test prion-like replication of the aggregation-prone conformation. In this experiment, [*trans*-MePro32]β2m served as a templating element, and the conformationally labile [F_2Pro32]β2m analogue was chosen as the receptive component. At neutral pH, freshly folded [F_2Pro32]β2m adopts a native-like structure as evidenced by its ^{1}H−^{15}N HSQC spectrum.[27] Solution ^{19}F NMR spectroscopy was used

DOI: 10.1021/ja510109p
J. Am. Chem. Soc. 2015, 137, 2524−2535

to monitor the *cis*/*trans* equilibrium of the F_2Pro32 residue in the presence and absence of [MePro32]β2m. Strikingly, upon prolonged incubation of the [MePro32]β2m:[F_2Pro32]β2m mixture, the fraction of the *trans*-F_2Pro32 conformer in the sample increased to 20% (Figure 7C), whereas considerably less isomerization was observed in the control sample lacking [MePro32]β2m. Although the insoluble precipitate that formed during incubation did not appear amyloid-like (Figure S14), it showed enhanced ThT fluorescence, suggesting an elevated cross-β structure content (Figure 7B). Previously, it was shown that adding the truncated ΔN6 β2m variant, which also favors the *trans*-Pro32 conformer, to wt β2m enhanced the dynamic properties of the protein on the μs-ms NMR time scale via bimolecular collisions and also increased its rate of aggregation at neutral pH.[23,68] In our study, transmission of the aggregation-prone conformation might occur analogously via bimolecular collisions or, alternatively, by conformational conversion of [*cis*-F_2Pro32]β2m to [*trans*-F_2Pro32]β2m within mixed [MePro32]β2m:[F_2Pro32]β2m oligomers.

In conclusion, detailed characterization of the chemically synthesized [MePro32]β2m derivative has provided strong evidence that constraining Pro32 in β2m into a *trans*-configuration generates an aggregation-prone protein. However, the molecular mechanism of amyloid formation is more complex than simple self-association of *trans*-Pro32 β2m conformers. Conformational dynamism of Pro32 influences all stages of the self-assembly process, including initial protein misfolding, amyloid nucleation, and subsequent propagation. From a practical perspective, since *trans*-[MePro32]β2m recapitulates the properties of transient β2m species in the initial steps of oligomerization, this conformationally stabilized protein molecule may serve as a convenient target for screening small-molecule and peptide binders or, alternatively, for selection of conformationally specific antibodies.[69] When identified, such molecules could be grafted onto dialysis membranes to trap misfolded β2m species in an attempt to ameliorate or prevent the development of complications of dialysis-related amyloidosis.

EXPERIMENTAL SECTION

Materials. Reagents for peptide synthesis were purchased from the same suppliers as described in our previous publication.[27] In addition, *O*-(7-azabenzotriazol-1-yl)-*N*,*N*,*N*′,*N*′-tetramethyluronium hexafluorophosphate (HATU) coupling reagent was bought from Aapptec. α-Methyl-L-proline was purchased from Bachem and Boc-protected according to a previously described protocol.[70] Synthesis of Boc-α-[^{13}C]methyl-L-proline was executed as reported before.[35] 8-Anilino-1-naphthalenesulfonic acid (ANS), rifamycin SV sodium salt, and thioflavin T (ThT) were purchased from Sigma-Aldrich.

Protein Chemical Synthesis. [MePro32]β2m, ^{13}C-labeled [$^{13}CH_3$Pro32]β2m, and ^{15}N-labeled (I7, V9, A15, G18, F22, V27, G29, F30, I35) [MePro32]β2m as well as [Gly32]β2m and [Aib32]β2m were chemically synthesized by "one-pot" native chemical ligation of three polypeptide fragments as reported previously.[27] When performing coupling of Boc-α-methyl-L-proline (Boc-MePro), Boc-α-[^{13}C]methyl-L-proline (Boc-[$^{13}CH_3$]Pro) or Boc-α-aminoisobutyric acid (Boc-Aib) in the synthesis of the corresponding (Thz25-Xaa32-Ala79).$^{\alpha}$SR middle fragments, HATU reagent was used instead of benzotriazole-*N*,*N*,*N*′,*N*′-tetramethyluronium hexafluorophosphate (HBTU). Product proteins were characterized by reverse-phase HPLC and high-resolution mass spectrometry (Figure S5 and Table S2). Mass spectrometric measurements were performed on a Bruker maXis ESI-Q-TOF or a Bruker Solarix ESI-FT-ICR instrument. Deconvolution of experimental mass spectrometric data was performed using the Zscore algorithm with the help of MagTran v1.03 software. The theoretical mass spectra were simulated using IsoPro v.3.0 software.

Protein Folding. Samples for NMR, CD, ANS binding, and proteolysis studies were prepared by dissolving lyophilized powder in 3 M guanidinium chloride, 0.1 M sodium phosphate, pH 7, and dialyzing it against 25 mM sodium phosphate buffer, pH 7.5, using a 3000 Da molecular weight cutoff dialysis membrane to remove denaturant. For protein oligomerization studies, lyophilized powder was directly dissolved in 50 mM sodium phosphate at pH 7, filtered through 0.2 μm membrane filters, and incubated at 25 °C.

NMR Spectroscopy. NMR samples were 0.15−0.4 mM protein in H_2O/D_2O (95%/5%), 25 mM sodium phosphate, 100 μM DSS-d_6, pH 7.5. Measurements were conducted in 3 mm Shigemi NMR tubes on a Bruker Avance III 600 spectrometer equipped with a cryo probe. The ^{1}H−^{13}C HSQC spectrum of the [$^{13}CH_3$Pro32]β2m analogue (Figure 2B) was acquired with 32 transients, spectral widths of 6009.65 Hz in F2 and 21 141.7 Hz in F1, with 2048 and 512 points in F2 and F1, respectively, with temperature set to 25 °C. The ^{1}H−^{15}N HSQC spectrum of ^{15}N-labeled [MePro32]β2m variant was acquired with 64 transients, spectral widths of 9615.4 Hz in F2 and 1946.3 Hz in F1 with 2048 and 512 points in F2 and F1, respectively. The temperature was set to 37 °C.

For wt β2m, the ^{1}H NOESY spectrum (τ_{mix} = 200 ms) was acquired with the spectral width set to 9615.4 Hz, where 16 transients of 2048 points per transient were obtained for each of the 512 t_1 increments (Figure 3F). For the [MePro32]β2m chemical analogue, the number of transients was increased to 64 due to attenuated signal intensity in order to obtain an NMR spectrum of the same quality as for the wild-type protein (Figure 3E). The temperature was set to 25 °C. Water suppression was achieved by excitation sculpting.

The ^{1}H−^{15}N TROSY spectra of [MePro32]β2m in the presence of rifamycin SV (Figure 6 E) were acquired with 64 transients, spectral widths of 9615.4 Hz in F2 and 1946.3 Hz in F1 with 2048 and 512 points in F2 and F1, respectively, with the temperature set to 37 °C. The data were processed using TopSpin software (v. 2) and analyzed with Sparky (v. 3.113) software.

The ^{19}F NMR data for [F_2Pro32]β2m ([protein] = 0.26 μM) and a mixture of [F_2Pro32]β2m ([protein] = 0.14 μM) and [MePro32]β2m ([protein] = 0.14 μM) (Figure 7) were recorded at 37 °C and referenced to the ^{19}F NMR signal of trifluoroacetic acid. For each spectrum, 30 000 transients were acquired with 56 818.2 Hz spectral width and 16 384 data points. The data were processed using TopSpin software (v. 2) and analyzed with MestReNova (v. 6.1) software.

Protein Oligomerization. Oligomerization studies on a 1:1 [MePro32]β2m:[F_2Pro32]β2m mixture and a [F_2Pro32]β2m control sample were performed directly in 3 mm Shigemi tubes used for NMR measurements. The proteins were incubated at 37 °C for a period of up to 2 months. A Shigemi tube design with an insertable plunger ensured confinement of the samples between glass surfaces and minimized the air−water interface, which is known to facilitate protein aggregation.[71] The larger air−solution interface in our previously reported experiments with [F_2Pro32]β2m, which were carried out in 1.5 mL Eppendorf tubes, resulted in a higher extent of oligomerization.[27]

Size Exclusion HPLC. Size exclusion HPLC reported in this work was performed on a YMC Pack Diol 200 column (250 × 4.6 mm, 200 Å, 5 μm) using 0.1 M potassium phosphate, 0.2 M NaCl buffer at pH 7.0, and flow rate of 0.5 mL/min. Small differences in elution volumes for different sets of experiments (i.e., in Figures 4, 6, and 7) are due to different HPLC instrumentation and small differences in hardware configuration (Waters Alliance 2695 and Dionex Ultimate 3000 RS instruments were used).

Monitoring Proteolysis Rates by SDS-PAGE. The wt β2m and [MePro32]β2m variants (c = 60 μM) were incubated in 25 mM sodium phosphate, 0.05% (w/v) NaN_3, pH 7.5, in the presence of trypsin (c = 7.5 μg/mL) at 25 °C. Aliquots were removed at different time points and analyzed by SDS-PAGE using PhastGel High Density acrylamide gels (GE Heathcare) and R350 Coumassie staining. Peptide markers from GE Healthcare were used to estimate molecular weights.

DOI: 10.1021/ja510109p
J. Am. Chem. Soc. 2015, 137, 2524−2535

ANS Binding Studies. Fluorescence of ANS (1-anilinonaphthalene-8-sulfonic acid) was measured at c = 10 μM ANS upon addition of 2 μM protein and incubation for 1 h in 25 mM sodium phosphate, pH 7.5. The excitation wavelength was set at 370 nm, and emission spectra were collected from 400 to 600 nm.

Circular Dichroism Spectroscopy. CD experiments were performed on an Aviv model 202 spectrometer for [MePro32]β2m and wt β2m. For measurements in the far-UV region (200−260 nm), the CD signal was recorded in a 2 mm path length cell using protein concentrations of 10−20 μM in 25 mM phosphate, pH 7.5 at 37 °C. Five wavelength scans with 0.5−1 nm step were collected and averaged. Thermal denaturation of the proteins was monitored by CD at 220 nm. The temperature was varied from 10 to 95 °C using 0.5 °C temperature steps, 2 min for temperature equilibration, and 1 min for CD signal averaging at each temperature step. Qualitative comparisons of thermal stability are based on apparent T_m values corresponding to a 50% change in ellipticity signal at 220 nm.

Amyloid Growth Experiments. In the typical conditions for amyloid growth (with or without seeding), protein was dissolved in 50 mM sodium citrate, 100 mM NaCl, pH 2.5 to a concentration of ∼50 μM and then filtered through 0.2 μm filter to remove any particulate material and dispensed into 1.5 mL Eppendorf tubes. Samples were then incubated at 37 °C with 250 rpm orbital shaking.

Growth kinetics experiments were performed on a Molecular Devices SpectraMax M2 platereader using Nunc black standard 96-well plates sealed with optically transparent films (ThermalSeal RT, Sigma). Fluorescence (ex. 455 nm, em. 485 nm) readings were performed every 5 min with shaking for 10 s between readings; reactions were monitored for up to 96 h. The temperature was set to 27 °C. Each well contained 100 μL of reaction solution comprising 40 μM protein, 50 μM ThT dye, and 2.5 μM amyloid seeds (total concentration of monomer) in 50 mM sodium citrate, 100 mM NaCl at pH 2.5.

For the preparation of seeds, 200 μL of amyloid solution grown for 2 weeks was centrifuged (14 000 rpm) at 4 °C for 1 h. Supernatant was then decanted, and fibrils were resuspended in the same volume of 50 mM sodium citrate, 100 mM NaCl, pH 2.5. The solution was then sonicated with a Hielscher Ultrasonics sonicator (UP 200S model) using a 3 mm microtip (MS3) with three 0.1-s pulses at 90 W/cm^2 acoustic power density.

Electron Microscopy. Formvar/carbon-coated 300 mesh copper EM grids were placed coated-side-down for 60 s onto sample drops containing the preformed β2m fibrils. The grids were then retrieved and briefly washed with deionized water, and the sample was stained with 2% (w/v) uranyl acetate for 20 s. Grids were then blotted and air-dried before analysis. Images were taken using a FEI Morgagni 268 or a Phillips CM12 electron microscopes operating at 100 keV.

ThT Fluorescence. ThT fluorescence (450 nm to 650 nm) was recorded on a PTI QM-7SE spectrofluorimeter using a 1.0 cm × 0.2 cm cuvette and an excitation wavelength of 440 nm. Aliquots of solutions containing protein oligomers or amyloids was added to 0.5 mL of ThT solution (c = 10 μM) in 25 mM sodium phosphate at pH 7.5.

MD Simulations. The simulations were carried out with the GROMOS biomolecular simulation package (http://www.gromos.net)[72−74] and the GROMOS force-field parameter set 54A7.[75] The initial coordinates for the simulations of the [*cis*-MePro32]β2m and [*cis*-Pro32]β2m conformers were derived from the crystal structure of wt β2m in the MHC1 complex (PDB ID: 2CLR). For the simulation of [*trans*-MePro32]β2m and [*trans*-Pro32]β2m conformers, the initial coordinates were based on the crystal structure of the H31F mutant (PDB ID: 3CIQ), in which the *trans*-Pro32 residue was replaced by *trans*-MePro in the case of the [*trans*-MePro32]β2m simulation (with Phe31 mutated back to His31). Each structure was solvated in a rectangular box of approximately 13 500 simple point charge (SPC) water molecules[76] with a minimal solute-to-wall distance of 1.2 nm resulting in a simulation box of approximately 41 700 atoms. To preserve the overall neutrality of the system two Na^+ ions were added. The simulations were performed using periodic boundary conditions at a constant temperature of 300 K and a constant pressure of 1 atm. Analysis of the trajectories was performed with the GROMOS++ suite of programs[77] using the configurations saved at 1 ps intervals. The stability of each protein during the simulation was assessed by analyzing the atom-positional RMSD from the energy-minimized initial structure (Figures 1D and S3) and the RMSF of the backbone N, C, and Cα atoms (Figures 1C and S3). Additionally, hydrogen bond analysis was performed to explore the reasons for differences in the structural stability of the *trans*- and *cis*-MePro32 conformers, respectively (Table S1). The occurrence of secondary structure elements as a function of time is presented in Figure S1 for simulations of [*cis*-MePro32]β2m and [*trans*-MePro32]β2m conformers and shows that the structure of all proteins is conserved during the course of MD simulations. The analysis of the His31-MePro32 Cα−N−C−Cα dihedral angle in [*cis*-MePro32]β2m and [*trans*-MePro32]β2m simulations presented in Figure S2 shows narrow and unimodal dihedral angle distributions with a mean value of −5.4° for the *cis*-MePro32 and 176.8° for the *trans*-MePro32. Further details of the simulation setup and analysis are provided in the Supporting Information.

■ ASSOCIATED CONTENT

Supporting Information

Analytical and spectroscopic characterization of proteins in the study, additional experimental data on proteolytic digestion, protein aggregation, and MD simulations. This material is available free of charge via the Internet at http://pubs.acs.org.

■ AUTHOR INFORMATION

Corresponding Author

*hilvert@org.chem.ethz.ch

Present Addresses

[§]V.T.: Institut de Science et d'Ingénierie Supramoléculaires, Université de Strasbourg, Strasbourg 67000, France

[∥]J.D.: Chemistry, Biology, Pharmacy Information Center, ETH Zurich, Zurich CH-8093, Switzerland

Notes

The authors declare no competing financial interest.

■ ACKNOWLEDGMENTS

We thank Prof. W. F. van Gunsteren for valuable advice and support on the MD simulations. Electron microscopy measurements were performed at the Electron Microscopy Center of the ETH Zurich (EMEZ). This work was generously supported by the ETH Zurich and an ETH Fellowship to V.T.

■ REFERENCES

(1) Chiti, F.; Dobson, C. M. *Annu. Rev. Biochem.* **2006**, *75*, 333−366.
(2) Greenwald, J.; Riek, R. *Structure* **2010**, *18*, 1244−1260.
(3) Jucker, M.; Walker, L. C. *Nature* **2013**, *501*, 45−51.
(4) Haass, C.; Selkoe, D. J. *Nat. Rev. Mol. Cell Biol.* **2007**, *8*, 101−112.
(5) Smith, D. P.; Ashcroft, A. E.; Radford, S. E. Hemodialysis-related amyloidosis. In *Protein Misfolding Diseases: Current and Emergent Principles and Therapies*; Ramirez-Alvarado, M., Kelly, J. M., Dobson, C. M., Eds.; John Wiley and Sons: Hoboken, NJ, 2010.
(6) Adams, E. J.; Luoma, A. M. *Annu. Rev. Immunol.* **2013**, *31*, 529−561.
(7) Floege, J.; Ketteler, M. *Kidney Int.* **2001**, *59*, 164−171.
(8) Heegaard, N. H. *Amyloid* **2009**, *16*, 151−173.
(9) Porter, M. Y.; Routledge, K. E.; Radford, S. E.; Hewitt, E. W. *PLoS One* **2011**, *6*, No. e27353.
(10) Verdone, G.; Corazza, A.; Viglino, P.; Pettirossi, F.; Giorgetti, S.; Mangione, P.; Andreola, A.; Stoppini, M.; Bellotti, V.; Esposito, G. *Protein Sci.* **2002**, *11*, 487−499.
(11) Eichner, T.; Radford, S. E. *J. Mol. Biol.* **2009**, *386*, 1312−1326.

DOI: 10.1021/ja510109p
J. Am. Chem. Soc. 2015, 137, 2524−2535

(12) Rennella, E.; Corazza, A.; Giorgetti, S.; Fogolari, F.; Viglino, P.; Porcari, R.; Verga, L.; Stoppini, M.; Bellotti, V.; Esposito, G. *J. Mol. Biol.* **2010**, *401*, 286−297.
(13) Yamamoto, S.; Hasegawa, K.; Yamaguchi, I.; Tsutsumi, S.; Kardos, J.; Goto, Y.; Gejyo, F.; Naiki, H. *Biochemistry* **2004**, *43*, 11075−11082.
(14) Platt, G. W.; Radford, S. E. *FEBS Lett.* **2009**, *583*, 2623−2629.
(15) Eichner, T.; Radford, S. E. *FEBS J.* **2011**, *278*, 3868−3883.
(16) McParland, V. J.; Kad, N. M.; Kalverda, A. P.; Brown, A.; Kirwin-Jones, P.; Hunter, M. G.; Sunde, M.; Radford, S. E. *Biochemistry* **2000**, *39*, 8735−8746.
(17) Barbet-Massin, E.; Ricagno, S.; Lewandowski, J. R.; Giorgetti, S.; Bellotti, V.; Bolognesi, M.; Emsley, L.; Pintacuda, G. *J. Am. Chem. Soc.* **2010**, *132*, 5556−5557.
(18) Debelouchina, G. T.; Platt, G. W.; Bayro, M. J.; Radford, S. E.; Griffin, R. G. *J. Am. Chem. Soc.* **2010**, *132*, 10414−10423.
(19) Debelouchina, G. T.; Platt, G. W.; Bayro, M. J.; Radford, S. E.; Griffin, R. G. *J. Am. Chem. Soc.* **2010**, *132*, 17077−17079.
(20) Eakin, C. M.; Berman, A. J.; Miranker, A. D. *Nat. Struct. Mol. Biol.* **2006**, *13*, 202−208.
(21) Jahn, T. R.; Parker, M. J.; Homans, S. W.; Radford, S. E. *Nat. Struct. Mol. Biol.* **2006**, *13*, 195−201.
(22) Lu, K. P.; Finn, G.; Lee, T. H.; Nicholson, L. K. *Nat. Chem. Biol.* **2007**, *3*, 619−629.
(23) Eichner, T.; Kalverda, A. P.; Thompson, G. S.; Homans, S. W.; Radford, S. E. *Mol. Cell* **2011**, *41*, 161−172.
(24) Esposito, G.; Michelutti, R.; Verdone, G.; Viglino, P.; Hernandez, H.; Robinson, C. V.; Amoresano, A.; Dal Piaz, F.; Monti, M.; Pucci, P.; Mangione, P.; Stoppini, M.; Merlini, G.; Ferri, G.; Bellotti, V. *Protein Sci.* **2000**, *9*, 831−845.
(25) Su, Y.; Sarell, C. J.; Eddy, M. T.; Debelouchina, G. T.; Andreas, L. B.; Pashley, C. L.; Radford, S. E.; Griffin, R. G. *J. Am. Chem. Soc.* **2014**, *136*, 6313−6325.
(26) Sakata, M.; Chatani, E.; Kameda, A.; Sakurai, K.; Naiki, H.; Goto, Y. *J. Mol. Biol.* **2008**, *382*, 1242−1255.
(27) Torbeev, V. Y.; Hilvert, D. *Proc. Natl. Acad. Sci. U.S.A.* **2013**, *110*, 20051−20056.
(28) Renner, C.; Alefelder, S.; Bae, J. H.; Budisa, N.; Huber, R.; Moroder, L. *Angew. Chem., Int. Ed.* **2001**, *40*, 923−925.
(29) Delaney, N. G.; Madison, V. *J. Am. Chem. Soc.* **1982**, *104*, 6635−6641.
(30) Welsh, J. H.; Zerbe, O.; von Philipsborn, W.; Robinson, J. A. *FEBS Lett.* **1992**, *297*, 216−220.
(31) Moretto, A.; Terrenzani, F.; Crisma, M.; Formaggio, F.; Kaptein, B.; Broxterman, Q. B.; Toniolo, C. *Biopolymers* **2008**, *89*, 465−470.
(32) De Poli, M.; Moretto, A.; Crisma, M.; Peggion, C.; Fromaggio, F.; Kaptein, B.; Broxterman, Q. B.; Toniolo, C. *Chem.—Eur. J.* **2009**, *15*, 8015−8025.
(33) Flores-Ortega, A.; Jiménez, A. I.; Cativiela, C.; Nussinov, R.; Aleman, C.; Casanovas, J. *J. Org. Chem.* **2008**, *73*, 3418−3427.
(34) Kang, Y. K.; Park, H. S. *New J. Chem.* **2014**, *38*, 2831−2840.
(35) Torbeev, V. Y.; Fumi, E.; Ebert, M.-O.; Schweizer, W. B.; Hilvert, D. *Helv. Chim. Acta* **2012**, *95*, 2411−2420.
(36) Fogolari, F.; Corazza, A.; Varini, N.; Rotter, M.; Gumral, D.; Codutti, L.; Rennella, E.; Viglino, P.; Bellotti, V.; Esposito, G. *Proteins: Struct., Funct. Bioinf.* **2011**, *79*, 986−1001.
(37) Routledge, K. E.; Tartaglia, G. G.; Platt, G. W.; Vendruscolo, M.; Radford, S. E. *J. Mol. Biol.* **2009**, *389*, 776−786.
(38) Woods, L. A.; Platt, G. W.; Hellewell, A. L.; Hewitt, E. W.; Homans, S. W.; Ashcroft, A. E.; Radford, S. E. *Nat. Chem. Biol.* **2011**, *7*, 730−739.
(39) Harper, J. D.; Lansbury, P. T. *Annu. Rev. Biochem.* **1997**, *66*, 385−407.
(40) Prusiner, S. B. *Science* **2012**, *336*, 1511−1513.
(41) Biancalana, M.; Koide, S. *Biochim. Biophys. Acta* **2010**, *1804*, 1405−1412.
(42) Kelly, J. W. *Curr. Opin. Struct. Biol.* **1996**, *6*, 11−17.
(43) Uversky, V. N.; Fink, A. L. *Biochim. Biophys. Acta* **2004**, *1698*, 131−153.
(44) Prusiner, S. B. *Proc. Natl. Acad. Sci. U.S.A.* **1998**, *95*, 13363−13383.
(45) Pan, K. M.; Baldwin, M.; Nguyen, J.; Gasset, M.; Serban, A.; Groth, D.; Mehlhorn, I.; Huang, Z.; Fletterick, R. J.; Cohen, F. E.; Prusiner, S. B. *Proc. Natl. Acad. Sci. U.S.A.* **1993**, *90*, 10962−10966.
(46) Cohen, F. E.; Pan, K.-M.; Huang, Z.; Baldwin, M.; Fletterick, R. J.; Prusiner, S. B. *Science* **1994**, *264*, 530−531.
(47) Deleault, N. R.; Harris, B. T.; Rees, J. R.; Supattapone, S. *Proc. Natl. Acad. Sci. U.S.A.* **2007**, *104*, 9741−9746.
(48) Wang, F.; Wang, X.; Yuan, C.-G.; Ma, J. *Science* **2010**, *327*, 1132−1135.
(49) Deleault, N. R.; Walsh, D. J.; Piro, J. R.; Wang, F.; Wang, X.; Ma, J.; Rees, J. R.; Supattapone, S. *Proc. Natl. Acad. Sci. U.S.A.* **2012**, E1938−E1946.
(50) Hill, A. F.; Antoniou, M.; Collinge, J. *J. Gen. Virol.* **1999**, *80*, 11−14.
(51) Wille, H.; Bian, W.; McDonald, M.; Kendall, A.; Colby, D. W.; Bloch, L.; Ollesch, J.; Borovinskiy, A. L.; Cohen, F. E.; Prusiner, S. B.; Stubbs, G. *Proc. Natl. Acad. Sci. U.S.A.* **2009**, *106*, 16990−16995.
(52) Stöhr, J.; Watts, J. C.; Mensinger, Z. L.; Oehler, A.; Grillo, S. K.; DeArmond, S. J.; Prusiner, S. B.; Giles, K. *Proc. Natl. Acad. Sci. U.S.A.* **2012**, *109*, 11025−11030.
(53) Lu, J. X.; Qiang, W.; Yau, W. M.; Schwieters, C. D.; Meredith, S. C.; Tycko, R. *Cell* **2013**, *154*, 1257−1268.
(54) Relini, A.; Canale, C.; DeStefano, S.; Rolandi, R.; Giorgetti, S.; Stoppini, M.; Rossi, A.; Fogolari, F.; Corazza, A.; Esposito, G.; Gliozzi, A.; Bellotti, V. *J. Biol. Chem.* **2006**, *281*, 16521−16529.
(55) Giorgetti, S.; Rossi, A.; Mangione, P.; Raimondi, S.; Marini, S.; Stoppini, M.; Corazza, A.; Viglino, P.; Esposito, G.; Cetta, G.; Merlini, G.; Bellotti, V. *Protein Sci.* **2005**, *14*, 696−702.
(56) Yamamoto, S.; Yamaguchi, I.; Hasegawa, K.; Tsutsumi, S.; Goto, Y.; Gejyo, F.; Naiki, H. *J. Am. Soc. Nephrol.* **2004**, *15*, 126−133.
(57) Borysik, A. J.; Morten, I. J.; Radford, S. E.; Hewitt, E. W. *Kidney Int.* **2007**, *72*, 174−181.
(58) Yamaguchi, I.; Suda, H.; Tsuzuike, N.; Seto, K.; Seki, M.; Yamaguchi, Y.; Hasegawa, K.; Takahashi, N.; Yamamoto, S.; Gejyo, F.; Naiki, H. *Kidney Int.* **2003**, *64*, 1080−1088.
(59) Hasegawa, K.; Tsutsumi-Yasuhara, S.; Ookoshi, T.; Ohhashi, Y.; Kimura, H.; Takahashi, N.; Yoshida, H.; Miyazaki, R.; Goto, Y.; Naiki, H. *Biochem. J.* **2008**, *416*, 307−315.
(60) Ookoshi, T.; Hasegawa, K.; Ohhashi, Y.; Kimura, H.; Takahashi, N.; Yoshida, H.; Miyazaki, R.; Goto, Y.; Naiki, H. *Nephrol. Dial. Transplant.* **2008**, *23*, 3247−3255.
(61) Pal-Gabor, H.; Gombos, L.; Micsonai, A.; Kovacs, E.; Petrik, E.; Kovacs, J.; Graf, L.; Fidy, J.; Naiki, H.; Goto, Y. *Biochemistry* **2009**, *48*, 5689−5699.
(62) Eakin, C. M.; Miranker, A. D. *Biochim. Biophys. Acta* **2005**, *1753*, 92−99.
(63) Srikanth, R.; Mendoza, V. L.; Bridgewater, J. D.; Zhang, G.; Vachet, R. W. *Biochemistry* **2009**, *48*, 9871−9881.
(64) Yamaguchi, I.; Hasegawa, K.; Takahashi, N.; Gejyo, F.; Naiki, H. *Biochemistry* **2001**, *40*, 8499−8507.
(65) Kihara, M.; Chatani, E.; Sakai, M.; Hasegawa, K.; Naiki, H.; Goto, Y. *J. Biol. Chem.* **2005**, *280*, 12012−12018.
(66) Myers, S. L.; Jones, S.; Jahn, T. R.; Morten, I. J.; Tennent, G. A.; Hewitt, E. W.; Radford, S. E. *Biochemistry* **2006**, *45*, 2311−2321.
(67) Kent, S. B. H. *Chem. Soc. Rev.* **2009**, *38*, 338−351.
(68) Karamanos, T. K.; Kalverda, A. P.; Thompson, G. S.; Radford, S. E. *Mol. Cell* **2014**, *55*, 214−226.
(69) Paduch, M.; Koide, A.; Uysal, S.; Rizk, S. S.; Koide, S.; Kossiakoff, A. A. *Methods* **2013**, *15*, 3−14.
(70) Khalil, E. M.; Subasinghe, N. L.; Johnson, R. L. *Tetrahedron Lett.* **1996**, *37*, 3441−3444.
(71) Campioni, S.; Carret, G.; Jordens, S.; Nicoud, L.; Mezzenga, R.; Riek, R. *J. Am. Chem. Soc.* **2014**, *136*, 2866−2875.
(72) Scott, W. R. P.; Hünenberger, P. H.; Tironi, I. G.; Mark, A. E.; Billeter, S. R.; Fennen, J.; Torda, A. E.; Huber, T.; Krüger, P.; van Gunsteren, W. F. *J. Phys. Chem. A* **1999**, *103*, 3596−3607.

DOI: 10.1021/ja510109p
J. Am. Chem. Soc. 2015, 137, 2524−2535

(73) Christen, M.; Hünenberger, P. H.; Bakowies, D.; Baron, R.; Bürgi, R.; Geerke, D. P.; Heinz, T. N.; Kastenholz, M. A.; Kräutler, V.; Oostenbrink, C.; Peter, C.; Trzesniak, D.; van Gunsteren, W. F. *J. Comput. Chem.* **2005**, *26*, 1719−1751.
(74) Schmid, N.; Christ, C. D.; Christen, M.; Eichenberger, A. P.; van Gunsteren, W. F. *Comput. Phys. Commun.* **2012**, *183*, 890−903.
(75) Schmid, N.; Eichenberger, A. P.; Choutko, A.; Riniker, S.; Winger, M.; Mark, A. E.; van Gunsteren, W. F. *Eur. Biophys. J.* **2011**, *40*, 843−856.
(76) Berendsen, H. J. C.; Postma, J. P. M.; van Gunsteren, W. F.; Hermans, J. Interaction models for water in relation to protein hydration. In *Intermolecular Forces*; Pullman, B., Ed.; Reidel: Dordrecht, The Netherlands, 1981; pp 331−342.
(77) Eichenberger, A. P.; Allison, J. R.; Dolenc, J.; Geerke, D. P.; Horta, B. A. C.; Meier, K.; Oostenbrink, C.; Schmid, N.; Steiner, D.; Wang, D.; van Gunsteren, W. F. *J. Chem. Theory Comput.* **2011**, *7*, 3379−3390.

DOI: 10.1021/ja510109p
J. Am. Chem. Soc. 2015, 137, 2524−2535